

Dual transmission filters for enhanced energy in mode-locked fiber lasers

Feng Li,¹ Edwin Ding,² J. Nathan Kutz,^{3,*} P. K. A. Wai¹

¹ Photonics Research Centre, Department of Electronic and Information Engineering, The Hong Kong Polytechnic University, Hung Hom, Kowloon, Hong Kong SAR, China

² Department of Mathematics and Physics, Azusa Pacific University, Azusa, CA 91702-7000, USA

³ Department of Applied Mathematics, University of Washington, Seattle, WA 98195, USA

*kutz@amath.washington.edu

Abstract: We theoretically demonstrate that in a laser cavity mode-locked by a set of waveplates and passive polarizer, the energy performance can be increased by incorporating a second set of waveplates and polarizer in the cavity. The two nonlinear transmission functions acting in combination can be engineered so as to suppress the multi-pulsing instability responsible for limiting the single pulse per round trip energy in a myriad of mode-locked cavities. In a single parameter sweep, the energy is demonstrated to double. It is anticipated that further engineering and optimization of the transmission functions by tuning the eight waveplates, fiber birefringence, two polarizers and two lengths of transmission fiber can lead to further significant increases. Moreover, the analysis suggests a general design and engineering principle that can potentially realize the goal of making fiber based lasers directly competitive with solid state devices. The technique is feasible and easy to implement without requiring a new cavity design paradigm.

© 2011 Optical Society of America

OCIS codes: (140.4050) Mode-locked lasers; (320.7090) Ultrafast lasers

References and links

1. D. J. Richardson, J. Nilsson, and W. A. Clarkson, "High power fiber lasers: current status and future perspectives," *J. Opt. Soc. Am. B* **27**, B63-B92 (2010).
2. H. A. Haus, "Mode-locking of lasers," *IEEE J. Sel. Top. Quant. Elec.* **6**, 1173-1185 (2000).
3. K. Tamura, E.P. Ippen, H.A. Haus and L.E. Nelson, "77-fs Pulse Generation From a Stretched-Pulse Mode-Locked All-Fiber Ring Laser," *Opt. Lett.* **18**, 1080-1082 (1993).
4. K. Tamura and M. Nakazawa, "Optimizing power extraction in stretched pulse fiber ring lasers," *Appl. Phys. Lett.* **67**, 3691-3693 (1995).
5. G. Lenz, K. Tamura, H. A. Haus, and E. P. Ippen, "All-solid-state femtosecond source at 1.55 μm ," *Opt. Lett.* **20**, 1289-1291 (1995).
6. F. Ö. Ilday, J. Buckley, and F. W. Wise, "Self-similar evolution of parabolic pulses in a laser cavity," *Phys. Rev. Lett.* **92**, 213902 (2004).
7. W. H. Renninger, A. Chong, and F. W. Wise. "Self-similar pulse evolution in an all-normal-dispersion laser," *Phys. Rev. A* **82**, 021805 (2010).
8. B. Bale and S. Wabnitz, "Strong spectral filtering for a mode-locked similariton fiber laser," *Opt. Lett.* **35**, 2466-2468 (2010).
9. A. Chong, W. H. Renninger, and F. W. Wise, "Properties of normal-dispersion femtosecond fiber lasers," *J. Opt. Soc. Am. B* **25**, 140-148 (2008).
10. S. Namiki, E. P. Ippen, H. A. Haus, and C. X. Yu, "Energy rate equations for mode-locked lasers," *J. Opt. Soc. Am. B* **14**, 2099-2111 (1997).
11. B. G. Bale, K. Kieu, J. N. Kutz, and F. Wise, "Transition dynamics for multi-pulsing in mode-locked lasers," *Opt. Express* **17**, 23137-23146 (2009).

12. E. Ding, E. Shlizerman and J. N. Kutz, "Generalized Master Equation for High-Energy Passive Mode-Locking: The Sinusoidal Ginzburg-Landau Equation," *IEEE J. Quantum Electron.* **47**, 705-714 (2011).
13. F. Li, P. K. A. Wai, and J. N. Kutz, "Geometrical description of the onset of multi-pulsing in mode-locked laser cavities," *J. Opt. Soc. Am. B* **27**, 2068-2077 (2010).
14. R. Herda, O. G. Okhotnikov, E. U. Rafailov, W. Sibbett, P. Crittenden, and A. Starodumov, "Semiconductor quantum-dot saturable absorber mode-locked fiber laser," *IEEE Photon. Technol. Lett.* **18**, 157-159 (2006).
15. S. Y. Set, H. Yaguchi, Y. Tanaka, and M. Jablonski, "Laser Mode Locking Using a Saturable Absorber Incorporating Carbon Nanotubes," *J. Lightwave Technol.* **22**, 51-56 (2004).
16. S. Yamashita, Y. Inoue, S. Maruyama, Y. Murakami, H. Yaguchi, M. Jablonski, and S. Y. Set, "Saturable absorbers incorporating carbon nanotubes directly synthesized onto substrates and fibers and their application to mode-locked fiber lasers," *Opt. Lett.* **29**, 1581-1583 (2004).
17. Z. Sun, T. Hasan, F. Torrisi, D. Popa, G. Privitera, F. Wang, F. Bonaccorso, D. M. Basko, and A. C. Ferrari, "Graphene Mode-Locked Ultrafast Laser," *ACS Nano* **4**, 803-810 (2010).
18. H. Zhang, "Large energy soliton erbium-doped fiber laser with a graphene-polymer composite mode locker," *Appl. Phys. Lett.* **95**, 141103 (2009).
19. H. Zhang, D. Y. Tang, L. M. Zhao, Q. L. Bao, and K. P. Loh, "Large energy mode locking of an erbium-doped fiber laser with atomic layer graphene," *Opt. Express* **17**, 17630-17635 (2009).
20. J. N. Kutz and B. Sandstede, "Theory of passive harmonic mode-locking using waveguide arrays," *Opt. Express* **16**, 636-650 (2008).
21. R. Devaney, *An Introduction to Chaotic Dynamical Systems*, 2nd ed. (Addison-Wesley, Redwood City, 1989).
22. P. G. Drazin, *Nonlinear systems*, (Cambridge, 1992)
23. C. R. Menyuk, "Pulse propagation in an elliptically birefringent Kerr media," *IEEE J. Quantum Electron.* **25**, 2674-2682 (1989).
24. C. R. Menyuk, "Nonlinear pulse propagation in birefringent optical fibers," *IEEE J. Quantum Electron.* **23**, 174-176 (1987).
25. A. Komarov, H. Leblond and F. Sanchez, "Multistability and hysteresis phenomena in passively mode-locked fiber lasers," *Phys. Rev. A* **71**, 053809 (2005).

1. Introduction

Over the past two decades, mode-locked fiber lasers have continued to show dramatic increases in performance and energy delivery. Indeed, a two orders of magnitude increase has been achieved only very recently [1] which pushes the output power to a comparable level with the solid state lasers. This pace of development has positioned fiber laser technologies as the potentially dominant paradigm for high-power/energy applications especially in the applications with size, weight and mobility requirements. Existing solid-state femtosecond lasers (exemplified by the ubiquitous titanium sapphire laser) are excellent laboratory tools, but instruments that are more stable and reliable, more user-friendly, and cheaper will allow application in a much broader range of settings; solid-state lasers rarely find application outside of research laboratories. These would include precision machining in manufacturing environments, biological imaging and surgical procedures in clinics, and even deployment in aircraft and our mobile facilities. Improved instruments will also greatly facilitate the use of femtosecond techniques in a wide range of scientific research, by i) allowing researchers to focus on the science of interest rather than operation of the short-pulse source, and ii) making short-pulse sources more available through reduced cost. Moreover, fiber lasers offer major practical advantages because light is contained in a waveguide, so careful alignment of an optical cavity is not required. The recent review article by Richardson *et al.* [1] gives an excellent review of the further advantages of fiber lasers.

To be more precise, one of the most commercially successful mode-locked lasers developed to date is a passive fiber laser cavity that uses a combination of waveplates and a passive polarizer for achieving saturable absorption [2] based on nonlinear polarization rotation (NPR). Laser cavities based upon this operating principle have evolved from delivering soliton-like mode-locking with pulse energies of approximately 0.1 nJ to delivering more exotic propagation behavior and mode-locking pulse shapes. In particular, dispersion-managed (stretched-pulse) soliton lasers deliver ≈ 1 nJ [3–5], similariton lasers peak around 10-20 nJ [6–8], and the

ANDi laser design [9] is capable of achieving energies of approximately 40 nJ.

With such new experimental insights, it is now realistic to design short-pulse fiber devices that compete directly with the existing solid state lasers in performance while offering major practical advantages at substantially reduced cost. However, the design and optimization of high-performance fiber devices is impeded by the so-called multi-pulsing instability (MPI) which ultimately imposes a fundamental limitation on a single mode-locked pulse energy [10–13]. To compete directly with solid state technologies, the final order-of-magnitude increase in energy is still required, thus making it critical to understand the limiting effects of the MPI and potential methods for suppressing it. Recently, some new techniques and materials, such as quantum dot doped fiber [14], carbon nanotubes [15, 16] and graphene [17–19] have been proposed to be adopted into the cavity as new type saturable absorbers. The compact new saturable absorbers based fiber lasers are promising candidates to enhance the pulse energy if the efficiency and damage threshold can be improved as promised in the coming years. But such lasers still require technological maturation before they can compete and be more broadly applied with the solid state lasers and NPR based fiber lasers. In this manuscript, we propose a feasible cavity modification that may enable significant performance enhancement without introduce any new materials or new techniques. Specifically, we propose engineering the cavity transmission characteristics by including a second set of waveplates and polarizer. Our theoretical model development and cavity simulations demonstrate the concept and show a promising avenue for such an approach for realistically suppressing MPI.

In this manuscript, we demonstrate that the insertion of a second set of waveplates and polarizer generates a second nonlinear transmission function which allows for suppression of the MPI phenomenon. The basic principle of operation is outlined in Sec. 2. In Sec. 3, a simplified geometrical model is developed that confirms the principle of operation and highlights the key features necessary for suppressing MPI. Full cavity simulations with the dual transmission functions are performed in Sec. 4 demonstrating that energy enhancement can indeed be achieved. The technological outlook for such methods of energy enhancement are considered in the conclusion Sec. 5.

2. Principle of Operation

The theoretical studies presented here are based upon integrating the key findings of two recent papers [12, 13]. Specifically, it is well known that the standard combination of waveplates and polarizer in a mode-locked cavity produces a periodic transmission curve. However, mode-locking models, such as the commonly accepted master equation [2], Taylor-expand the transmission curve so as to include only the first transmission window as a function of intensity. In Ref. [13], a geometrical description was developed showing that proper engineering of the transmission curve could allow mode-locking to naturally occur on the higher transmission windows instead of going through the MPI. However, this first manuscript did not connect such an idealized transmission curve with a physically realistic cavity design. Concurrently, Ref. [12] showed that the master equation need not be truncated through a Taylor expansion. Rather, the entire physics of the nonlinear, periodic transmission could be retained in the mode-locked cavity equations so as to match the physically realizable system. In this second paper, it was demonstrated that higher-energy mode-locked solutions could indeed be stable. However, higher-energy states were not obtained from a cold cavity (noise) startup.

Integrating the qualitative dynamics of the geometrical approach [13] with the full cavity dynamics with periodic transmission [12], a model is developed here demonstrating a practical way to achieve the necessary transmission curve which is capable of suppressing MPI and pushing the instability out to much higher energy levels. Specifically, it is suggested that a second set of waveplates, fiber, and polarizer be inserted into the cavity so that two distinct sinusoidal

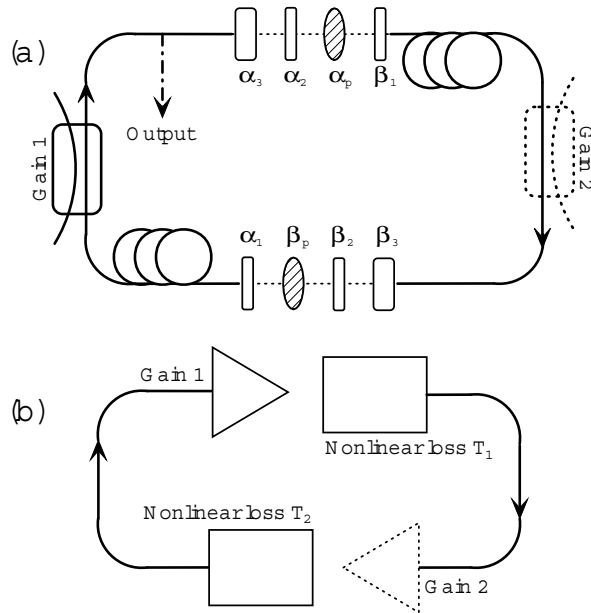


Fig. 1. (a) Experimental configuration of a generic ring cavity laser that includes four quarter-waveplates ($\alpha_1, \alpha_2, \beta_1, \beta_2$), two half-waveplates (α_3, β_3), two passive polarizers (α_p, β_p), and one or two ytterbium-doped amplifiers. The Yb-doped and standard single-mode fiber sections are fused together and the gain will be treated distributed. The birefringence of each fiber section can be adjusted by the coiled polarization controllers. The waveplate and polarizer angles (α_j, β_j) can all be measured accurately in experiment. (b) Idealization of the physical cavity with T_1 and T_2 representing the nonlinear, periodic transmission functions generated from the waveplate and polarizers. Transmission T_1 is generated from the α parameters while T_2 is generated from the β parameters. In both configurations, the second gain element are optional. It can be inserted to adjust the effective T_2 curve if needed.

transfer functions can be combined to form a more sophisticated transfer function. In particular, the combination of two transfer functions, denoted by T_1 and T_2 , are capable of producing an MPI suppressing behavior. Figure 1 demonstrates the physical setup that captures the fundamental principle expounded. In Fig. 1(a), a physically realizable cavity is shown with two sets of waveplates and polarizers. Each of these sets generates a nonlinear, periodic transmission T_1 and T_2 respectively. An idealization of the cavity is shown in Fig. 1(b) where the waveplate and polarizer dynamics is replaced by the transmission functions T_1 and T_2 . In both Fig. 1(a) and (b), the second gain elements are optional in the systems. It can be adopted to amplify the pulse after the first NPR set which will enhance the nonlinearity of the second NPR set effectively and compensate the cavity loss while needed. But this gain element is not considered in the simulations of this paper.

Two specific theoretical studies are performed in this manuscript: one corresponding to the full cavity dynamics of Fig. 1(a), and one corresponding to the simplified dynamics of Fig. 1(b). Of critical importance is the effect of the two, versus one, transmission curves. In particular, the overall cavity transmission curve as a function of the electric field energy E will be approximated by the combination

$$T(E) = T_2(T_1(E)E)T_1(E) \quad (1)$$

where $T(E)$ is the effective transmission curve generated from the successive application of T_1

and T_2 . It is this flexibility that allows for the creation of the ideal transmission curves suggested for overcoming MPI [13].

3. Dual transmission filter dynamics: a geometrical viewpoint

The most insightful way to consider the effects of dual transmission curves in the cavity is through a geometrical model developed by Li *et al.* [13] that builds upon the formulation of Namiki *et al.* [10]. This model assumes the cavity takes the simplified form shown in Fig. 1(b). In this model, the mode-locked pulse energy is computed over one round trip. The exact waveform of the mode-locked pulse is not considered. The geometrical model is a highly idealized model that is derived under a wide array of assumptions. As such, it can only possibly show some qualitative results and demonstrate new principles. It certainly cannot produce an accurate description of the laser output. Regardless, the model has been highly successful, in our view, in highlighting many of the key features associated with MPI and its suppression. As will be shown in the following sections, the predictions made with the model hold in the full cavity simulation dynamics.

Two primary components of laser dynamics are considered: the nonlinear loss (transmission) and the saturating gain. The saturating gain dynamics is modeled by the following differential equation [2, 13]:

$$\frac{dE_j}{dZ} = \frac{g_0}{1 + \sum_{j=1}^N E_j/E_{sat}} E_j \quad (2)$$

where E_j is the energy of the j th potential pulse ($j = 1, 2, \dots, N$) in a round trip of the cavity, g_0 is the gain coefficient which determine the small signal gain, and E_{sat} is the saturation energy determined by the pumping power of the cavity. The total gain in a round trip of the cavity can be controlled by adjusting the parameters g_0 or E_{sat} . The cavity energy can be increased by simply increasing the saturation energy E_{sat} . Adjusting g_0 can normally see equivalent and similar behavior in the cavity. The model is very generic and can be applied to many types of laser cavities just with adjusting the parameters. This equation can be exactly solved with standard methods of differential equations. However, the resulting solution is in implicit form which can only be determined numerically.

In addition to the saturating gain, nonlinear losses in the cavity are generated by the transmission functions T_1 and T_2 via the combination of waveplates, polarizer and fiber propagation. The nonlinear loss in the cavity, i.e. the saturable absorption or saturation fluency curve, will be modeled by a transmission function:

$$E_{out} = T(E_{in})E_{in} \quad (3)$$

where E_{in} and E_{out} are the input and output energies respectively of the transmission function T . Here we assume that the width of the mode locked pulses propagating in the cavity will not vary significantly so the pulse energy will be proportional to the peak power approximately. In the geometrical model, it is necessary to describe the pulse by a common parameter in the gain element and IDL to capture the straightforward insight. So we use the pulse energy which is assumed proportional to the peak power of the pulses here to target a clear insight of the mechanism that enhances the pulse energy with some loss of accuracy. To affirm the findings from the geometrical model, we will use a sophisticate model to perform some simulations with enough accuracy in Sec. 4. In experiments, the actual form of the transmission function $T(E_{in})$ for different system can vary significantly, especially with very high energies input. And in the case of interest here, two transmission curves are considered.

To be more precise about the overall transmission curve $T(E)$, individual transmission curves T_1 and T_2 are considered. Guided by the findings of Ref. [13], we construct the two transmission

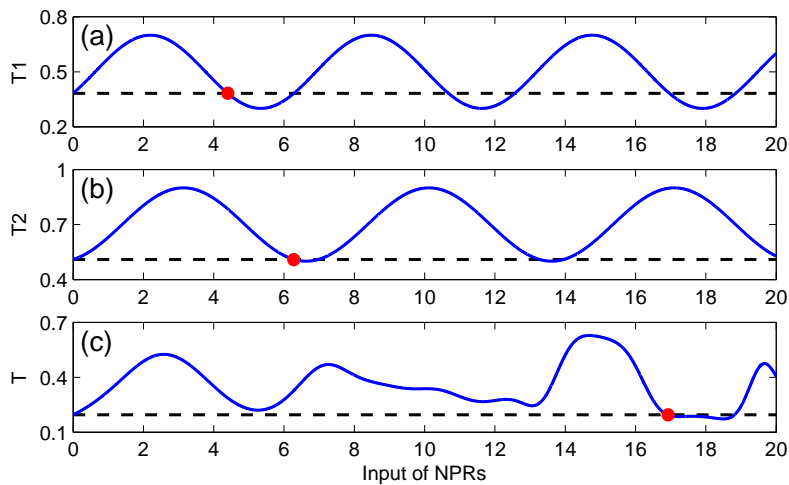


Fig. 2. The individual performance of the first, (a) T_1 , and second, (b) T_2 , nonlinear transmission functions generated by the waveplates and polarizer acting in combination. The parameter T is the combined transmission function, (c) $T_2(T_1(E)E)T_1(E)$. The dotted line in the bottom of each figure is the multipulse transition threshold, which is the small signal transmission of the illustrated transmission function. By enlarging the region that the transmission function stays above this curve, the single pulse energy can be significantly enhanced [13] since the multipulsing threshold (red dots) can be pushed out from (a) 4.4 and (b) 6.3 to (c) 16.9.

curves

$$T_1(E) = 0.5 - 0.2\cos(1.0E + 0.3\pi) \quad (4a)$$

$$T_2(E) = 0.7 - 0.2\cos(0.9E + 0.1\pi). \quad (4b)$$

Such transmission curves can be prescribed by the combination of polarizer, waveplates, cavity length and birefringence settings in the cavity [12]. Indeed, reverse engineering the cavity design based upon this simple geometrical model is the overarching goal of this and future studies. Note that even in the region that the MPI instability can be suppressed, the pulse may still bifurcate to periodic or chaotic mode-locked states [20].

The overall transmission curve is then prescribed by Eq. (1). Figure 2 demonstrates the two transmission curves T_1 and T_2 along with their effective cavity transmission curve T . Note that the two individual transmission curves are designed with carefully chosen periods and phase shift so as to create the overall transmission depicted in Fig. 2(c). The dotted lines show the small signal transmission of the functions given by $T_1(0)$, $T_2(0)$ and $T(0)$. From the geometrical model, MPI will be triggered at the first point that the transmission drop to lower than the small signal transmission, ie, the MPI threshold [13]. The transmission functions T_1 and T_2 can be carefully chosen to enlarge the region that the composite transmission function can stay above the threshold line.

In the simulations to characterize the multi-pulsing transition dynamics and bifurcation in the cavity, the saturable gain Eq. (2) as a function of the pulse number will be estimated with the engineered effective transmission curve shown in Fig. 2(c). The process are simply performed as shown in Fig. 1(b). By passing the saturating gain and nonlinear losses alternatively, we can obtain an iterative map for which only pulses with gain loss balance can be stabilized and

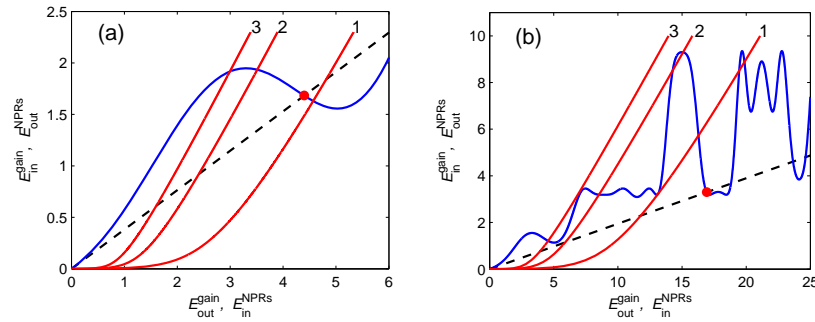


Fig. 3. The saturating gain and nonlinear loss (effective transmission) curves of the laser cavity with single NPR (a) and dual NPRs(b). The blue solid lines are the output/input of $T_1(E)$ defined in Eq. (4) and $T(E)$ in Eq. (1). The black dotted lines are the multipulse transition thresholds defined same as Fig. 2. The red curves are saturable gain curves for the cases of 1-pulse, 2-pulse or 3-pulses per round trip. The red dot at the cross point of the loss curves and threshold line are the threshold points of multi-pulsing. The laser output will be determined by the cross points of gain and loss curves. Note that before the cross point of the 1-pulse gain curve and loss curve reaches the threshold points, there will be only one pulse in the cavity. With the increase of E_{sat} , the 1-pulse solution point will pass the threshold which will trigger the multi-pulsing which will lead to the 2-pulse solutions in the cavity. The 1-pulse gain curve in (b) also shows the transition point from stable solutions to chaotic solutions. Note that the laser cavity in (b) has much larger threshold than in (a) which can afford much larger single pulse energy before the multi-pulse transition. The parameters used here are identical to those of Fig. 2 with the saturable gain $g_0 = \log(1000)$ which correspond to small signal gain 30 dB. The fiber length of the gain is 1 meter. Here (a) $E_{sat} = 0.5$ and (b) $E_{sat} = 1.8$.

survive in the cavity. Specifically, the output of the gain is the input of the nonlinear loss and vice-versa. This type of iterative maps are very similar to the logistic map which has a rich set of dynamics can be observed with a simple nonlinearity [21, 22]. Indeed, the multi-pulsing system can show qualitatively similar behavior to the logistic map with steady-state, periodic and chaotic behavior all potentially observed in practice [13]. Such behaviors are consistent with full cavity simulations [20].

Thus for mode-locking operation, the intersection of the effective transmission curve with the saturating gain curves for one, two, three or more pulses per round trip are the only possible stable mode-locked states. Figure 3 shows the effective transmission curves (blue lines) along with the saturating gain curves (red lines) for 1-pulse, 2-pulse and 3-pulse mode-locking operation. The black dash straight lines are the small signal loss line (threshold line) determined by $T_1(0)E$ and $T(0)E$. In case that the gain loss cross point is lower than the threshold line, the small signal will see smaller loss than the large pulse signal, that means the small signals (e.g. noises) in the cavity will have larger net gain than the existed pulses. So the small signals will be amplified to larger signals and eventually form more pulses in the cavity. Fig. 3(a) shows the gain and loss curves with the function T_1 defined by Eq. (4a) corresponding to a single NPR in the cavity. With the increase of E_{sat} , the gain curves will shift toward right side. The cross points of the gain and loss curves will climb along the loss curve. Since the black threshold line has a cross point (the red point) with the blue nonlinear loss curve in the first period of it, the solution point will trigger the multi-pulsing before it reach the second period of the loss curve. So the largest single pulse energy can be obtained with the cavity defined in Fig. 3(a) is limited by the red point. In Fig. 3(b), the blue nonlinear loss curve is the response with the composite loss

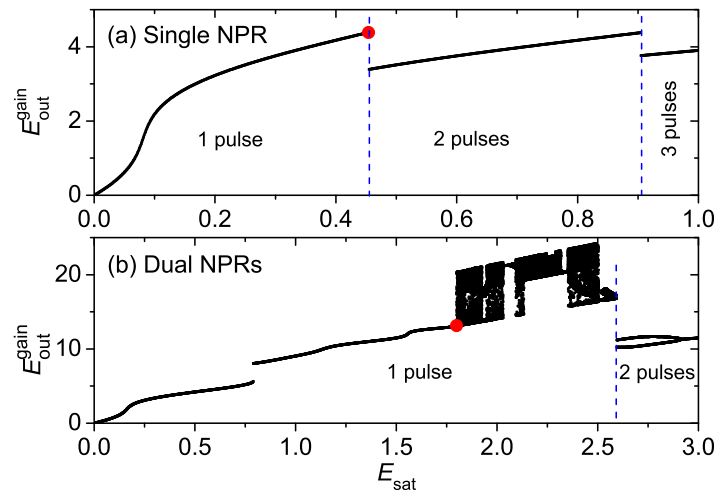


Fig. 4. The pulse energy per pulse with the increase of E_{sat} . The upper panel (a) is for the cavity with a single transmission function for generating nonlinear polarization rotation (NPR), and the bottom panel is for dual NPRs. The cavity parameters are the same as those used in Fig. 3. With a single NPR, the pulse energy will trigger the multi-pulse transition (red dot) at energy of approximately 4. The dual NPR cavity remains stable (red dot) up to an energy of approximately 13 before generating chaotic solutions. Thus the dual transmission can enhance the pulse energy by a factor of three. The blue vertical dash lines indicate the multi-pulse transition points.

defined by Eqs. (1), (3) and (4). The first cross point (red point) of the blue nonlinear loss curve and the threshold line is extended far from the first period of the nonlinear loss. Multi-pulsing can be suppressed in this broad region before the red point. We should note that bifurcation and chaos still can occur in this broad region while the loss curve has large slope [13].

Figure 4 demonstrates the simulation results with the iterative process outlined in Li *et al.* [13] for two key cases: a single transmission curve, i.e. only one set of waveplates and polarizers for generating nonlinear polarization rotation, and the dual transmission curve of Fig. 3 as illustrated in Fig. 1(b). Figure 4(b) clearly demonstrates that the multi-pulsing instability is suppressed by the proper engineering of the dual transmission curve. Indeed, a nearly 200% increase in performance can be achieved before the onset of chaotic dynamics. Given the tremendously large parameter space afforded by practical experiments, it is anticipated that this performance enhancement can be further increased. In contrast, Fig. 4(a) shows that a single transmission curve quickly trigger the multi-pulsing once the single pulse energy reaches the MPI threshold point defined by the red points in Fig. 2(a) and Fig. 3(a). To understand this enhancement more clearly, we can interpret its results by a specific example. Assume that: (i) the pulse shape (width) is not significantly altered per round trip so that the output pulse width is approximately 100fs; (ii) The cavity length is assumed to be composed of 20m of optical fiber with a nonlinearity coefficient of $2\text{W}^{-1}\text{km}^{-1}$; and (iii) The doped fiber will provide small signal gain 30dB. Then the laser pulse output will be limited to 33nJ while the peak power is 330W before triggering the multi-pulsing instability. After we insert the second NPR set, this energy limitation can be enhanced to about 100nJ with 200% improvement.

The simple geometrical arguments and theory expounded here build upon previous findings [13] by suggesting a practical way of generating a nonlinear transmission curve capable of

suppressing MPI. Indeed, the dual transmission is a simple and elegant way of engineering the requisite transmission. In the next section, full cavity simulations demonstrate that the simple engineering principle of transmission curve design indeed produces performance enhancement.

4. Full laser cavity dynamics with dual transmission

The simulations with the geometrical model in Section 3 has shown promising enhancement to the pulse energy with another set of NPR in the laser cavity. The simulations are based on such a generic geometrical model which can be applied in most types of mode locked laser but loss some important features of specific fiber laser cavities such as dispersion and nonlinearity. The results from the geometrical model can only show the qualitative results to demonstrate the working principle of the enhancement by the additional NPR. But since the performance of such fiber laser systems can be affected by the neglected features significantly, it's necessary to perform full simulations with a sophisticate model for such cavities. To affirm the theoretical predictions of the simplified model of the previous section, full simulations of the laser cavity shown in Fig. 1(a) are performed. The governing equations in the j -th fiber section are given by coupled nonlinear Schrödinger equations (CNLS) [12, 23, 24]:

$$i \frac{\partial u}{\partial z} + \frac{D_j}{2} \frac{\partial^2 u}{\partial t^2} - K_j u + (|u|^2 + A|v|^2) u + Bv^2 u^* = iR_j u, \quad (5a)$$

$$i \frac{\partial v}{\partial z} + \frac{D_j}{2} \frac{\partial^2 v}{\partial t^2} + K_j v + (|v|^2 + A|u|^2) v + Bu^2 v^* = iR_j v, \quad (5b)$$

where

$$R_j = \frac{2g_{0,j}}{1 + (\|u\|^2 + \|v\|^2)/e_{0,j}} \left(1 + \tau_j \frac{\partial^2}{\partial t^2} \right) - \Gamma_j. \quad (6)$$

In the above system, u and v represent the two orthogonally polarized electric field envelopes in an optical fiber with birefringence K_j . The z coordinate denotes the propagating distance normalized by the length of the first fiber section, and t denotes the retarded time normalized by the full-width at half-maximum of the pulse. D_j is the averaged group velocity dispersion of the j -th fiber section (doped and undoped fiber sections), and is positive for anomalous dispersion and negative for normal dispersion. In the ANDi laser which we consider in this paper, D is always negative [9]. The nonlinear coupling parameters A (cross-phase modulations) and B (four-wave mixing) are determined by the material of the optical fiber. In axial symmetrical fibers, $A + B = 1$ will be satisfied and, specific values $A = 2/3$ and $B = 1/3$ [23, 24] are adopted in normal single mode fibers. The dissipative terms, R_j , accounting for the saturable, bandwidth limited saturating gain and attenuation, In particular, $g_{0,j}$ and $e_{0,j}$ are the nondimensional pumping strength and the saturating energy of the gain respectively for each section of fiber. The parameter τ_j characterizes the bandwidth of the pump, and Γ_j measures the distributed losses caused by the output coupling and the fiber attenuation. Note that $\|u\|^2 = \int |u|^2 dt$ and $\|v\|^2 = \int |v|^2 dt$ denote the energy in each of the orthogonally polarized electric field components where integration is for $t \in [-\infty, \infty]$.

The effect of the waveplates and passive polarizer can be modeled by the corresponding Jones matrices [12, 25]. The standard Jones matrices of the quarter-waveplate, half-waveplate and polarizer are given, respectively, by

$$W_{\frac{\lambda}{4}} = \begin{pmatrix} e^{-i\pi/4} & 0 \\ 0 & e^{i\pi/4} \end{pmatrix}, \quad (7a)$$

$$W_{\frac{\lambda}{2}} = \begin{pmatrix} -i & 0 \\ 0 & i \end{pmatrix}, \quad (7b)$$

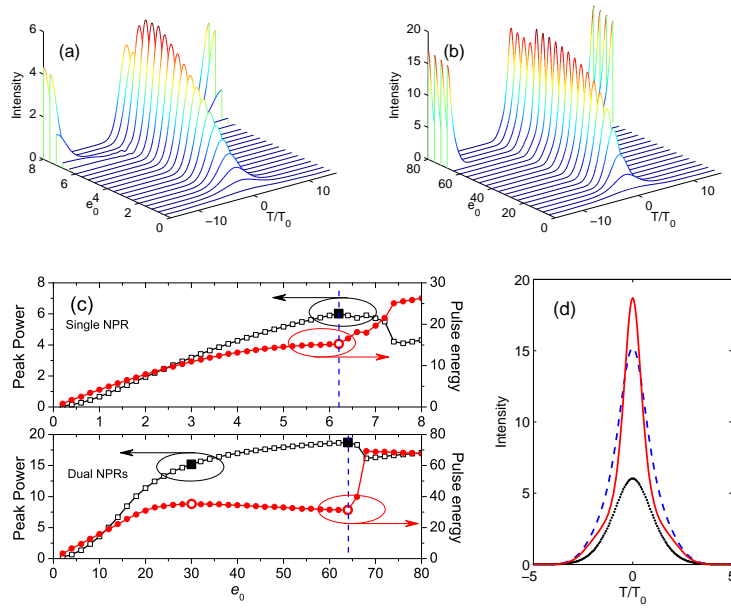


Fig. 5. The stable mode-locked pulse shape is shown as a function of increasing saturation energy $e_{0,j}$ in (a) for a single NPR laser cavity and (b) for a dual NPRs laser cavity. Panel (c) shows the pulse peak power and energy variation with $e_{0,j}$ for both lasers. The vertical blue lines indicate the multi-pulsing transition threshold. In the top panel of (c), the line with square marks shows the peak power and the line with circle marks shows the pulse energy. The zoomed solid square and hollow circle at $e_{0,1} = 6.2$ indicate the maximum peak power and pulse energy that can be obtained in this laser. There are two pair of zoomed marks in the bottom panel of (c). The left pair marks at $e_{0,1} = 30$ show the pulse with maximum pulse energy and the right pair marks at $e_{0,1} = 64$ show the pulse with maximum peak power. The three pulses indicated by the three pair zoomed marks are shown in (d). The black dot line shows the pulse with maximum energy and peak power obtained in single NPR system shown in (a) and the top panel of (c). The blue dash line/red solid line shows the pulse with maximum energy/peak power in dual NPR system shown in (b) and the bottom panel of (c). The parameters of the single NPR system are $\alpha_1 = 0$, $\alpha = 0.49\pi$, $\alpha = 0.2\pi$, $\alpha_p = 0.45\pi$, $K_1 = 0.1$, $D_1 = -0.4$, $\tau_1 = 0.1$, $\Gamma_1 = 0.1$, $g_{0,1} = 1.73$ and $e_{0,1}$ is varied. The parameters in the dual NPR system are same as the single NPR system only except that the variables $g_{0,2} = 0$ and $e_{0,2} = 0$, which means the second NPR set is passive. Other parameters of the second set NPR are same to the first set.

$$W_p = \begin{pmatrix} 1 & 0 \\ 0 & 0 \end{pmatrix}. \quad (7c)$$

These matrices are valid only when the principle axes of the devices are aligned with the fast axis of the fiber. For arbitrary orientation α_j ($j = 1, 2, 3, p$) shown in Fig. 1, the matrices are modified according to

$$J_j = R(\alpha_j)WR(-\alpha_j), \quad (8)$$

where W is the Jones matrix of the device given in Eq. (7) and R is the rotation matrix

$$R(\alpha_j) = \begin{pmatrix} \cos \alpha_j & -\sin \alpha_j \\ \sin \alpha_j & \cos \alpha_j \end{pmatrix}. \quad (9)$$

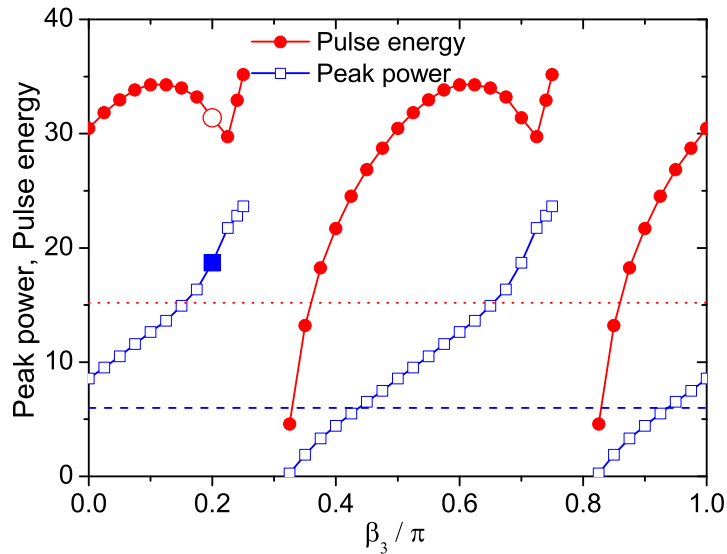


Fig. 6. The peak power (blue line with square marks) and pulse energy (red line with circle marks) with the maximum $e_{0,1}$ without triggering the multipulsing at different β_3 in dual NPRs cavity. The red dot line and blue dash line are the maximum pulse energy and peak power can be obtained in single NPR cavity. The zoomed blue square and red circle marks correspond to the results with dual NPRs in Fig. 5.

The governing evolution equations (5) together with Jones matrices (8) gives a full description of pulse propagation in the laser system. The principle of operation involves iterations of solving the CNLS over one round trip and applying the Jones matrices of the waveplates and polarizer consecutively. The discrete application of Jones matrices after each cavity round trip acts like a filter that can be tuned to control the mode-locking behavior. Indeed, they are responsible for generating the nonlinear transmission functions T_1 and T_2 . Depending on their orientations, the waveplates and the polarizer can either destabilize the field propagating in the cavity or lock it into a particular polarization component so that robust mode-locking can be achieved.

Simulations of the full cavity dynamics and mode-locking for normal dispersion are shown in Fig. 5 for both a single and dual transmission configuration. In both cases stable mode-locking is achieved. However, the maximum performance using two sets of waveplates and polarizers gives a significant increase in energy delivery. In simulations, we first find a stable mode locking setting of the waveplates and polarizer. Then we increase the saturation energy of the gain $e_{0,1}$ slightly. The pulse peak power and energy will both increase till the multipulsing been triggered with $e_{0,1} > 6.2$. The maximum pulse peak power and energy can be obtained with these parameters are 6.0 and 15.2 as shown in Fig. 5(a). Then we add one more set of fiber, waveplates and polarizer into the cavity. The second set parameters are same to the first set shown in Fig. 5(a) except $g_{0,2} = 0$. Then $e_{0,1}$ is varied again as shown in Fig. 5(b). With the dual NPRs setting, the peak power and pulse energy can be enhanced to 18.7 and 31.4 before the multipulsing been triggered while $e_{0,1} > 64$. The peak power and pulse energy variation with the increase of $e_{0,1}$ in both cavity settings are shown in Fig. 5(c). Note that with dual NPRs

in the cavity, the maximum pulse energy 35.2 is obtained at $e_{0,1} = 30$ which is not the point with maximum peak power. The pulse waveforms with maximum peak power or energy in both settings are shown in Fig. 5(d). The significant peak power and pulse energy enhancement found in this sophisticated model is consistent with the discrete, geometrical model of the last section.

To understand how to achieve maximal performance as a function of one of the parameters, a simple parameter space sweep is performed. Given the overwhelmingly large parameter space represented by the waveplates and polarizers, we will focus on this one parameter sweep in order to illustrate the dual transmission concept. Figure 6 performs a sweep of the parameter through varying the values of β_3 from 0 to π . This one parameter sweep of a dual transmission laser cavity illustrates the peak power and pulse energy with the maximum $e_{0,1}$ without triggering the multipulsing at different β_3 . Note that the pulse energy shown in the figure are not always the maximum value that can be obtained with the given β_3 value. This is already known from Fig. 5(c). The maximum peak power and pulse energy from single NPR cavity is also drawn on the Figure for comparison. Note that while β_3 is tuned to about 0.3π or 0.8π , stable solution can not be obtained. It is obvious that the second set of NPR can enhance the pulse energy and peak power in most region of β_3 .

5. Conclusions

Modeling and simulation are powerful tools in helping design next generation fiber lasers. It is through theoretical studies that we can suggest concrete techniques for suppressing the ubiquitous MPI limitations and potentially increase pulse energies a final order of magnitude in order to compete directly with solid state lasers. Indeed, it is a clear goal of the fiber laser community to surpass solid state performance in this current decade. Here, a simple yet effective technique is demonstrated for enhancing mode-locked energy delivery, namely a second set of waveplates and polarizer are applied to the cavity with the desired second transmission curve capable of suppressing MPI. Although the results are far from the desired order-of-magnitude increase, it does suggest a clear method by which MPI and pulse energies can be easily increased. By varying only a single parameter, an increase of 100% was easily achieved.

In ongoing investigations, it is our intent to use these simple design principles to design and engineer transmission functions capable of much larger energy enhancements. One of the primary difficulties in the theoretical modeling is the effort required to connect the desired transmission curves T_1 and T_2 (each of which has a few degrees of freedom describing its period, modulation depth, and offset) to the full cavity model and its large parameter space determined by the waveplates ($\alpha_1, \alpha_2, \alpha_3, \beta_1, \beta_2$ and β_3), the polarizers α_p and β_p , the fiber lengths (L_1 and L_2), the fast-slow axis alignments, and birefringence K_1 and K_2 . This requires the engineering and nonlinear mapping of a 14-dimensional parameter space to generate the desired transmission curve $T(E)$ that has a periodic structure and whose troughs remain above the small signal gain limit [13]. Although at first such a large parameter sweep seems rather daunting, it also suggests that there is a great deal of flexibility in engineering almost any periodic transmission curve desired, thus potentially allowing for upwards of an order of magnitude increase in energy if mode-locking can be achieved on the third, fourth or higher period of the periodic transmission window.

Acknowledgments

P. K. A. Wai and Feng Li acknowledge the support of the Research Grant Council of the Hong Kong Special Administrative Region, China (project PolyU5282/11E). J. N. Kutz acknowledges support from the National Science Foundation (NSF) (DMS-1007621) and the U.S. Air Force Office of Scientific Research (AFOSR) (FA9550-09-0174).